THE ASTROPHYSICAL JOURNAL, 352:55–67, 1990 March 20

IMAGES IN THE ROCKET ULTRAVIOLET: STAR FORMATION AND EXTINCTION IN THE M51 SYSTEM

RALPH C. BOHLIN
Space Telescope Science Institute
ROBERT H. CORNETT AND JESSE K. HILL
ST Systems Corporation
ROBERT W. O'CONNELL[1]
University of Virginia
AND
THEODORE P. STECHER
Laboratory for Astronomy and Solar Physics, Goddard Space Flight Center
Received 1989 July 5; accepted 1989 September 16

ABSTRACT

UV images of M51 with up to 15″ resolution were obtained by a rocket-borne telescope. The bandwidth was 970 Å with maximum response at 2650 Å. The two most prominent features of M51 in the UV are the bright central region and a region of intense star formation about 2.5 NE of the nucleus toward the companion NGC 5195. This complex is the source of 20% of the total UV flux in M51. The companion is much less prominent in the UV than in optical bands. Spiral arms show much higher contrast in UV and *U* bands than in the *R* band. The nuclear region in the UV band shows clumped emission from probable star-forming regions, possibly associated with the inner Lindblad resonance. These regions are probably the UV counterparts of FIR sources discovered in an EW scan across the nucleus. UV/*U* colors of most bright H II regions with known extinction are consistent with O star spectra reddened by amounts estimated from radio and Balmer line measurements. However, some of the brightest H II regions have redder UV/*U* colors, probably indicating the presence of cooler stars which contribute in the *U* band. CO and IR observations indicate that the companion NGC 5195 may be a reddened starburst in spite of its faintness in the UV.

Subject headings: galaxies: individual (M51) — galaxies: structure — ultraviolet general

I. INTRODUCTION

Ultraviolet images of spiral galaxies are dominated by the luminous hot stars present in regions of active star formation; consequently, the ultraviolet imaging of spiral galaxies is a powerful technique for mapping stellar populations and interstellar dust (Bohlin *et al.* 1982; Hill, Bohlin, and Stecher 1984). Starbursts appear in high contrast in the ultraviolet since older, cooler populations disappear (Bohlin *et al.* 1983). The large-scale morphology of star-forming regions stands out uniquely, and may therefore most easily be studied, in ultraviolet images.

We observed the Sbc(s)I–II spiral galaxy NGC 5194 (M51) and its companion NGC 5195 on the same rocket flight that was used to observe M101 (Stecher *et al.* 1982; Hill, Bohlin, and Stecher 1984). During the flight, thermal effects on the payload caused a drift in alignment between the telescope and the pointing system which diminished during the course of the flight. M101, observed with less drift during the latter part of the flight, was therefore studied first. Since that work was done, significant enhancements in the speed and flexibility of our image processing software and hardware have made treatment of the M51 data feasible.

In § II we describe the observations and data reduction of the UV images as well as those of the ground-based images used for comparison. In § III we discuss the large-scale features, in § IV H II regions and other isolated sources, and in § V, the nuclear region of M51. M51's companion galaxy NGC 5195 is discussed in § VI, followed by a summary in § VII.

II. OBSERVATIONS AND DATA REDUCTION

a) UV Images

The rocket payload was launched from White Sands Missile Range at 5:00 UT 1979 May 21 on Astrobee 25.043. It consisted of a 31.1 cm diameter f/5.6 Ritchey-Chrétien telescope with an electrostatically focused ITT microchannel plate image intensifier coupled to Kodak IIa-O film, as described by Bohlin *et al.* (1982). The bandpass was defined by the response of the CsTe photocathode with a calcium fluoride filter to eliminate geocoronal Lyα emission. The vital statistics of the instrumental system are given in Table 1 of Hill, Bohlin, and Stecher (1984).

Four exposures on M51 were made, one of 6 s duration and three of 50 s, after which the pointing was moved to M101. The spatial resolution was limited by the stability of the pointing system to 10 × 15 arcsec on the 6 s exposure; the greater thermal drift of the telescope with respect to the gyroscopic platform limited the long exposures to 10 × 40 arcsec resolution.

Hill, Bohlin, and Stecher (1984) have described the payload's bandpass calibration procedure. The bandwidth is 970 Å with the maximum response for a flat spectrum source at a wavelength of 2650 Å. The effective wavelength of the payload, for the flux distribution of NGC 5471 as determined by *IUE* observations, is 2250 Å.

[1] Visiting Astronomer, Kitt Peak National Observatory, National Optical Astronomy Observatories, which is operated by the Association of Universities for Research in Astronomy, Inc., under contract with the National Science Foundation.

All flight frames and laboratory calibration images were digitized on a PDS 1010a microdensitometer using a 20 μm square aperture, resulting in 2048 × 2048 pixel density images. The images were processed with the Ultraviolet Imaging Telescope (UIT) Batch Data Reduction (BDR) software system. Details of the system and its use on UIT data, which are similar to that from this flight, are in Cornett, Hill, and Hill (1987) and Hill (1987). The images were corrected for drift of the PDS response with time, adjusted to a uniform fog level, converted to (linear) relative exposure units, and flat-fielded using the BDR system. The conversion to relative intensity and flat-fielding is estimated from the reproducibility of the sky level and the brightest sources to be accurate to ±15% over a dynamic range of about 100 in exposure.

Astrometric parameters for the rocket images were derived in batch mode by the BDR system. Point sources were located using UITPHOT, a version of DAOPHOT (Stetson 1987) adapted for UIT, and an approximate plate solution derived previously was refined by automatically identifying UITPHOT sources with astrometric standards from the Space Telescope Guide Star catalog (Lasker and McLean 1987). The final plate solution has a formal error of 2–3 arcsec, which is the positional uncertainty in the UV images. UITPHOT was also used to perform aperture photometry on sources from selected lists (see § IV).

The absolute calibration for the payload was determined by using *IUE* spectra of H II regions in M101 as standards to compare with the results of aperture photometry from the images. A later check of the absolute calibration, consisting of comparing the UV flux of M51 from the rocket exposures for the regions observed by *ANS* and *OAO* with the values obtained by those instruments, shows a difference of 35%. We now believe that this discrepancy is due to the fact that some of the flux of the M101 H II regions falls outside the *IUE* aperture; therefore all of the fluxes in Hill, Bohlin, and Stecher (1984) should be multiplied by 1.35. The relative values remain the same.

Further processing was performed interactively in MOUSSE (Multi-Option UIT Software System Environment) (Landsman and Pfarr 1989) using MOUSSE and special-purpose IDL software for interactive image manipulation and display.

b) Ground-based Images

Ground-based images of M51 were obtained on 1985 April 18 with an RCA C33063 two-stage image tube on the Kitt Peak National Observatory no. 3 0.4 m telescope. The telescope and image tube combination were chosen to match as closely as possible the resolution and dynamic range characteristics of the Ultraviolet Imaging Telescope. Two exposures each were obtained on IIIa-J emulsion in the *U* band (UG2 + $CuSO_4$, λ(peak) = 3670 Å) and *R* band (Mould R12-1267, λ(peak) = 6480 Å). Exposure times were 1.5 and 4.5 minutes in *U* and 1.0 and 3.0 minutes in *R*. The FWHM of stellar images resulting from combined resolution, seeing, and guiding effects was ~10 arcsec.

Digitization and fog level adjustment of the ground-based images were similar to that for the rocket images. Spot sensitometer plates were taken to monitor processing quality, but the images were linearized by requiring frames in each bandpass with different exposure times to give consistent photometric results for sources of all brightnesses. A single characteristic curve was found to give good results for both bandpasses. The images were not flat-fielded. From comparisons of aperture photometry from our images with similar results derived by Schweizer (1976) the photometric accuracy of the ground-based images, including linearization and field-flatness errors, is estimated to be 25%.

Astrometric parameters were derived interactively using MOUSSE. Because of S-distortions introduced by the image intensifier, astrometric reference stars were employed only from a subset of the field near the center; the resultant plate solutions have formal errors of 2–3 arcsec. All rocket- and ground-based images were rotated to north-up, east-left orientation and adjusted, using bilinear interpolation, to a common plate scale using MOUSSE. Further analysis was performed interactively on that system.

III. LARGE-SCALE FEATURES

Figure 1*a* shows the blue POSS image of M51 (with a 2′ radius circle centered on the nucleus). Figure 1*b* shows the 6 s UV exposure of the M51 system. Figures 1*c*–1*d* show the 270 s *U* and 180 s *R* ground-based exposures. The two most prominent features in the UV are the bright central region within about 30″ of the nucleus and the northeast complex (NEC), a region of intense star formation at a radial distance of 2–3 arcmin. The interacting companion NGC 5195 is much less prominent in the UV than in the optical bands.

The total fluxes of M51 in the UV, *U*, and *R* bands are 5.5×10^{-13}, 8.4×10^{-13}, and 1.2×10^{-12} ergs (cm^2 Å s)$^{-1}$, respectively. These fluxes were computed using circular apertures centered on the nucleus of radius 3′, after subtracting a modal sky brightness, as in DAOPHOT. The total fluxes of NGC 5195 in the three bands were determined in a similar way using a 70″ radius aperture. The UV, *U*, and *R* fluxes are 1.5×10^{-14}, 8.9×10^{-14}, and 3.3×10^{-13} ergs (cm^2 Å s)$^{-1}$, respectively.

a) Radial Surface Brightness Profiles

Hill, Bohlin, and Stecher (1984) presented UV radial surface brightness profiles of the young arm and old disk components of M101, derived from images obtained on the same rocket flight as the M51 UV data discussed here. They also summarized earlier optical observations of the photometric structure of disk galaxies.

Elmegreen and Elmegreen (1984) presented azimuthally averaged surface brightness profiles of 34 spiral galaxies, including M51, determined from digitized ground-based images in the *B* (blue) and *I* (near-infrared) bands. Boroson (1981) also produced radial profiles in the *B* band for a sample of 26 spiral galaxies, including M51. Where possible, Boroson fit the profiles to a two-component bulge plus exponential disk model. We have determined, and plotted in Figure 2, azimuthally averaged radial surface brightness profiles of M51 in the UV, *U*, and *R* bands.

The UV, *U*, and *R* profiles are qualitatively similar. They are dominated by a nuclear component for $r < 50''$ and a flat disk component for $50'' < r < 150''$, with a more rapid decline in flux for $r > 150''$. Because of the changes in profile slope, M51 is one of nine spiral galaxies out of 26 whose radial profile Boroson (1981) was unable to fit using his bulge plus exponential disk model. The M51 radial profiles are quite unlike the M101 radial profile discussed by Hill, Bohlin, and Stecher (1984). The M101 UV radial profile could be fitted by an exponential disk alone with no additional nuclear component and

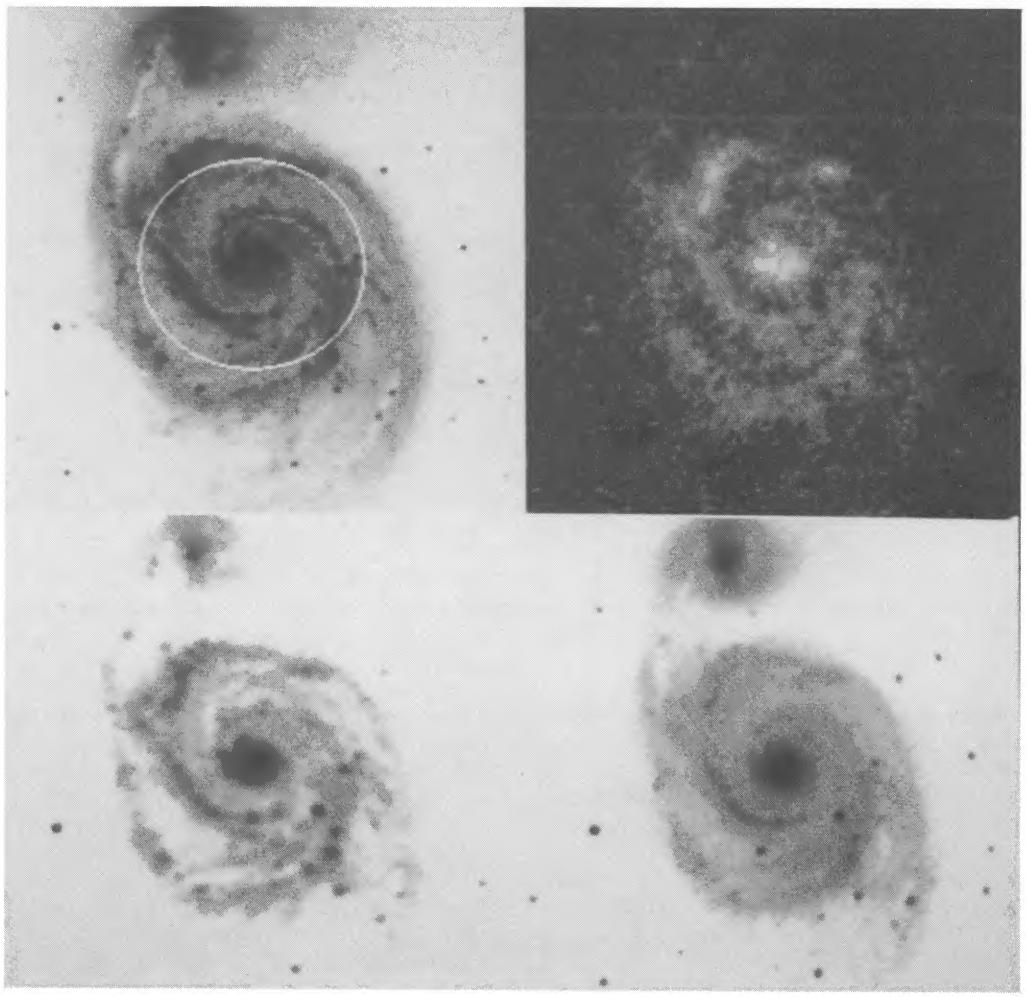

FIG. 1.—10′ × 10′ fields centered near on M51 in four bands. (*a*) Palomar Observatory Sky Survey blue plate. The radius of the circle is 2′; (*b*) 6 s rocket UV image; (*c*) 270 s ground-based U image; (*d*) 180 s ground-based R image. North is at the top and east is at the left.

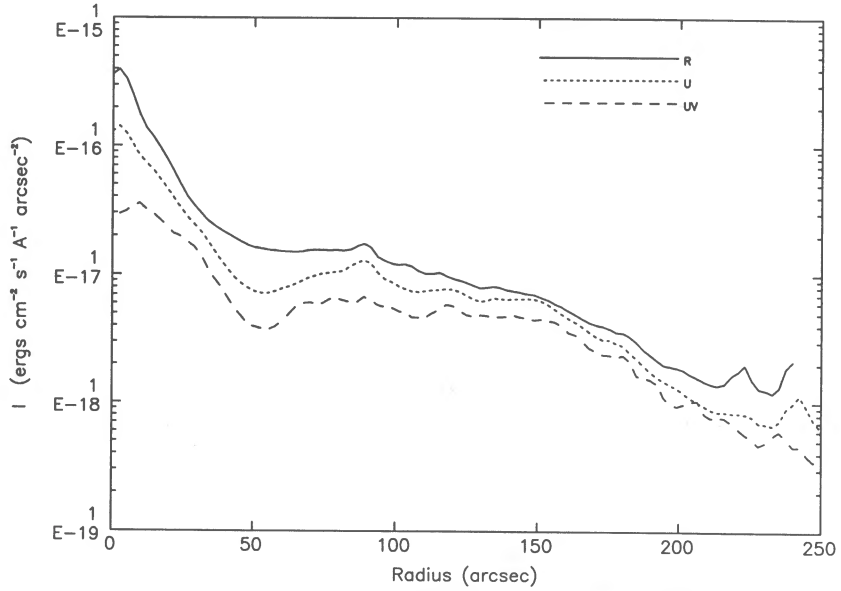

FIG. 2.—I_{uv}, I_u, and I_r azimuthally averaged radial profiles for M51

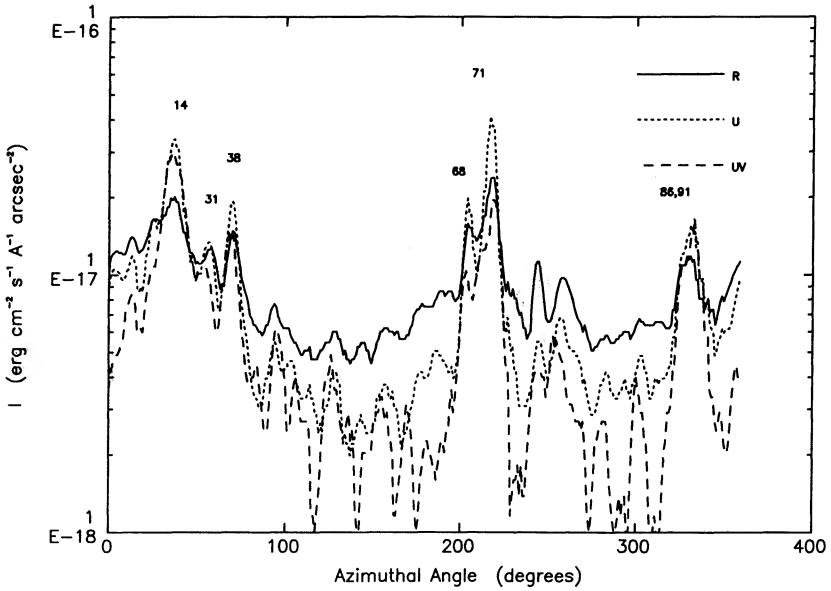

FIG. 3.—I_{uv}, I_u, and I_r azimuthal profiles for radius 136″. The positions of prominent CCM H II regions are indicated. The azimuthal angle is measured counterclockwise from N in degrees.

no faster decline apparent at large radii. A comparison of large-scale UV features of M51 and M101 is made in § III*e*).

A comparison of the UV and *U* profiles in Figure 2 suggests a large-scale radial color gradient, in which $I_{uv}(r)/I_u(r)$ increases with increasing radius. We find that the gradient is sharp near the nucleus, with $I_{uv}(r)/I_u(r)$ increasing from 0.2 to 0.6 as the radial distance r increases from 0 to 30 arcsec. The radial increase in $I_{uv}(r)/I_u(r)$ then becomes more gentle, increasing to about 0.75 at $r = 150$ arcsec, and decreasing slowly for larger radii.

Inspection of an I_{uv}/I_u map shows that $I_{uv}/I_u = 0.4$–0.6 in interarm regions, while areas of intense star formation may have I_{uv}/I_u as high as 1.5. The observed radial color gradients in I_{uv}/I_u and I_u/I_r can then be attributed to a radially increasing fraction of the disk flux from star-forming regions out to a radius of about 150″.

b) Azimuthal Surface Brightness and Ratio Plots

Elmegreen and Elmegreen (1984) presented azimuthal relative surface brightness profiles in the *B* and *I* bands at radii 102, 136, and 170 arcsec. We have determined azimuthal profiles for our calibrated UV, *U*, and *R* band images at the same radii. The surface brightness profiles for radius 136″ are plotted in Figure 3. Some of the brightest star-forming regions, including part of the NEC, are found at this radius. The corresponding azimuthal I_u/I_r ratio plot is given in Figure 4. The UV rocket image has a broader PSF than the ground-based images. Therefore, quotients involving I_{uv} are not shown, since

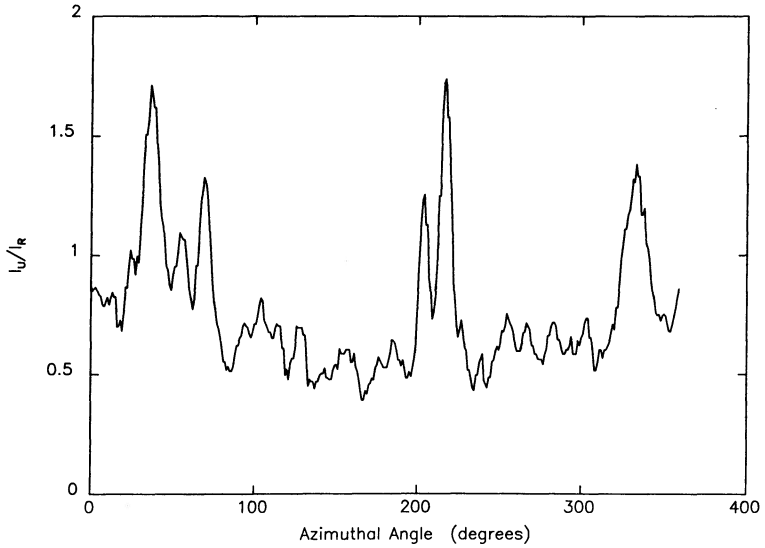

FIG. 4.—I_u/I_r azimuthal profile at $r = 136''$

they have spurious features where the surface brightness changes rapidly. The images were filtered with a 12″ box before extracting the profiles to decrease the small scale noise, so the effective width of the profiles is 12″.

We find that the brightest (nonstellar) peaks in the azimuthal profiles in all bands are positionally coincident with H II regions identified by Carranza, Crillon, and Monet (1969, hereafter CCM), as indicated in Figure 3. Hill, Bohlin, and Stecher (1984) found a similar result for the M101 UV data, where most of the peaks in the azimuthal profiles could be identified with discrete UV sources coincident with H II regions previously found from optical data. The spiral arm sources of both M51 and M101 show greater peak-to-trough contrast in the UV azimuthal profiles than in the optical profiles obtained by Schweizer (1976).

Neither galaxy has peaks in the azimuthal profiles that can be identified with representative cross sections through fairly uniform spiral arms. Instead, the peaks are identifiable with individual OB/H II complexes along the tightly wrapped spiral arms.

c) *Surface Brightness Scans*

In addition to the radial and azimuthal profiles discussed above, we have extracted profiles for two representative scans through the nucleus of M51. The UV, U, and R images were boxfiltered by 12″ before extracting the profiles. Burkhead (1978) scanned photoelectrically in U, B, and V along the same directions.

i) *E-W Scan through the Center of M51*

The first scan follows an east-to-west path through the M51 nuclear complex at a constant declination. The I_{uv}, I_u, and I_r profiles for this scan are shown in Figure 5. The ratio profile I_u/I_r is shown in Figure 6.

The nuclear source (centered at $x = 0$) appears broader for shorter wavelengths. The greater width of the I_{uv} and I_u profiles is mostly due to a blended spiral arm source just east of the nucleus. This component is faint in the R profile, stronger relative to the nucleus in the U profile, and as strong as the nuclear component in the UV. Weaker westward components are present as well. The eastern source is clearly visible in Figure 5, and is associated with H II region CCM 43B. The UV scan shows a shallow relative minimum at the location of the maxima of the U and R scans. The UV minimum is flanked by two maxima separated by about 20″. This structure and its relation to similar structures found in other bandpasses will be discussed in § V.

The strong secondary peaks in all three bands about 1.′5 to the east and west of the nucleus show where the scan crosses the major spiral arms. The spiral arm crossings coincide with local maxima of I_u/I_r (see Fig. 6). In the R band broad density waves in the old disk population (Schweizer 1976) are of lower amplitude than in the U band. The narrower U arms mostly arise from younger, earlier type stars.

ii) *Scan Connecting M51, NGC 5195*

The second scan follows a line inclined 15° east of north, connecting the nuclei of M51 and NGC 5195. The surface brightness profiles for this scan are shown in Figure 7. The corresponding I_u/I_r profile is given in Figure 8.

The two most important additional features in the second scan are the crossing of the NEC star-formation complex at $x = 150''$ and the nucleus of NGC 5195 at $x = 250''$. Both the U and UV scans peak strongly at the NEC, while the R scan rises gently toward the maximum point, then falls abruptly. I_u/I_r peaks in this region as well.

The nucleus of the interacting companion NGC 5195 is detected as a strong maximum in all three bands. The height of the peak relative to the peak associated with the nucleus of M51 diminishes with decreasing wavelength. Extended emission is detected over arcmin scales in all bands. The faint UV peaks on either side of the nucleus coincide with similar features visible in the U image with lower contrast. We believe that extinction within M51 and NGC 5195 itself accounts for the apparently red colors of the nucleus compared with that of M51 and for the faintness of the extended UV emission. The UV emission from the companion is treated at greater length in § VI.

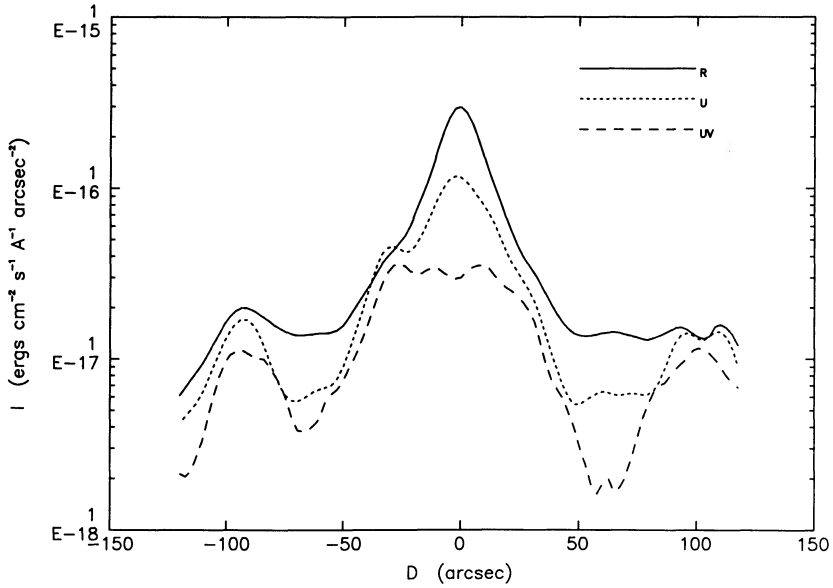

FIG. 5.—I_{uv}, I_u, and I_r profiles for an E-W scan through the nucleus of M51

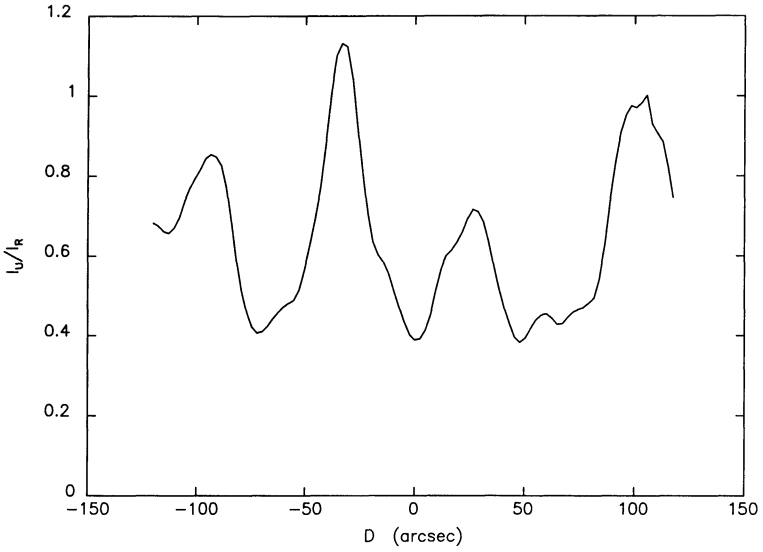

FIG. 6.—I_u/I_r profile for an E-W scan through the nucleus of M51

d) The NEC

The NEC is a region of intense star formation located about 2'.5 northeast of M51's nucleus toward NGC 5195. It extends about 2' along a spiral arm. Many bright H II regions are located here, including CCM 8, 10, 14, 19, and 27. We estimate the total UV flux of the NEC in our band at 9.8×10^{-14} ergs $(\text{cm}^2\ \text{Å}\ \text{s})^{-1}$, or 0.18 of the total UV flux of the galaxy.

Estimating the *U* and *R* fluxes of the NEC in the same way as the UV flux gives 1.1×10^{-13} ergs $(\text{cm}^2\ \text{Å}\ \text{s})^{-1}$ for both, so all three bands give essentially the same flux. This region is significantly bluer than the galaxy as a whole, since only 14% of the total M51 U flux and 9.5% of the total *R* flux originate in the NEC. The spectrum of the NEC is apparently essentially flat from about 2500 Å to 7000 Å.

O-type stars must be common in the NEC, from the presence of many bright H II regions. We infer that the observed flat spectrum is heavily influenced by dust or contains many cooler B and A stars in addition to the O stars, probably both. The effects of dust and a mixed stellar population could, in principle, be disentangled from spectrophotometric measurements. Ground-based extinction measurements will be combined with F_{uv}/F_u measurements of the H II regions to partially investigate this question in § IV.

e) UV Comparison of M51 and M101

M101, the other galaxy observed on the same rocket flight, has quite different spiral structure from that of M51. Unlike

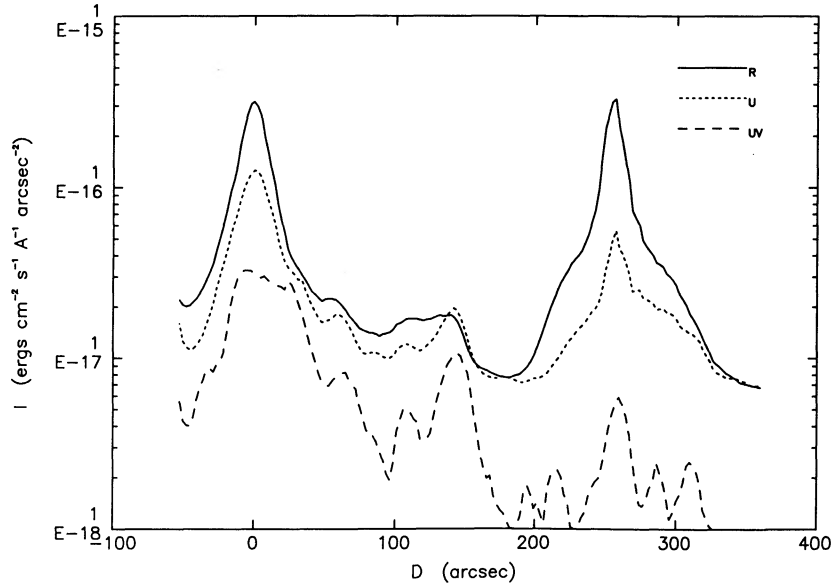

FIG. 7.—I_{uv}, I_u, and I_r profiles for a S-N scan inclined 15° E of N, and connecting the nuclei of M51 and NGC 5195

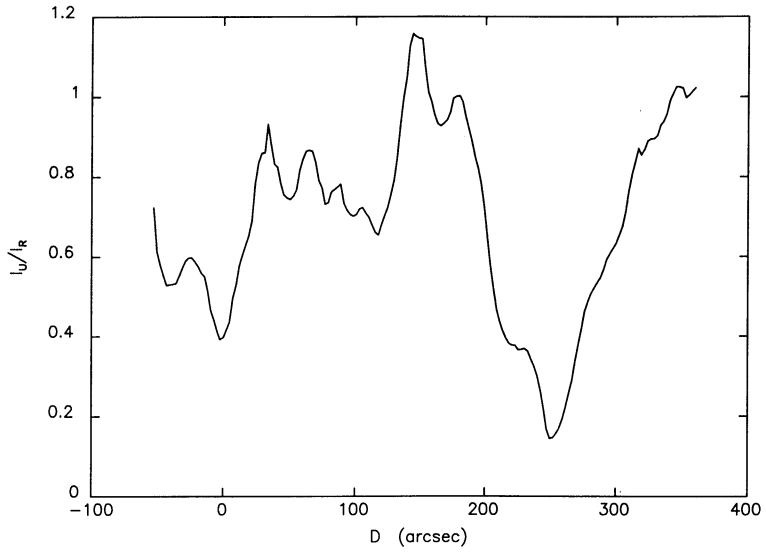

FIG. 8.—I_u/I_r profile for an S-N scan connecting M51, NGC 5195 nuclei

M51, M101 has no inner Lindblad resonance, and does not have strong differential rotation (Kormendy and Norman 1979). It does not have a symmetric two-armed grand design spiral structure, as does M51. M101 has no closely interacting companion of comparable mass, although the small galaxy NGC 5477 may have influenced the faint arms discussed by Stecher *et al.* (1982).

Although the global F_u/F_r ratio, as determined from ground-based images taken with the same telescope and detector as the M51 ground-based images, is somewhat lower than that of M51 (0.5 vs. 0.7), F_{uv}/F_u is slightly higher (0.8 vs. 0.7). The shapes of the radial surface brightness profiles are quite different, as shown in Figure 9, where we have computed radial distances using the distances 7.2 Mpc (M101) and 9.6 Mpc (M51) (Sandage and Tammann 1974). The M51 profile plotted in Figure 9 was computed using the sum of the three 50 s exposures.

As mentioned earlier, the M101 radial profile is well described by a power law, with scale length 4.5 kpc, over its entire range, while the M51 profile is not well described by a single power law (Boroson 1981). The surface brightness of the outer regions of M51 decreases much more rapidly with distance than in M101.

From the similarity in F_{uv}/F_u and F_u/F_r colors, there is no evidence from our images that M101 has a much stronger O-type population than M51. Since M101 is one of the galaxies with high supernova rate discussed by Richter and Rosa (1989), but M51 is not, this is somewhat surprising.

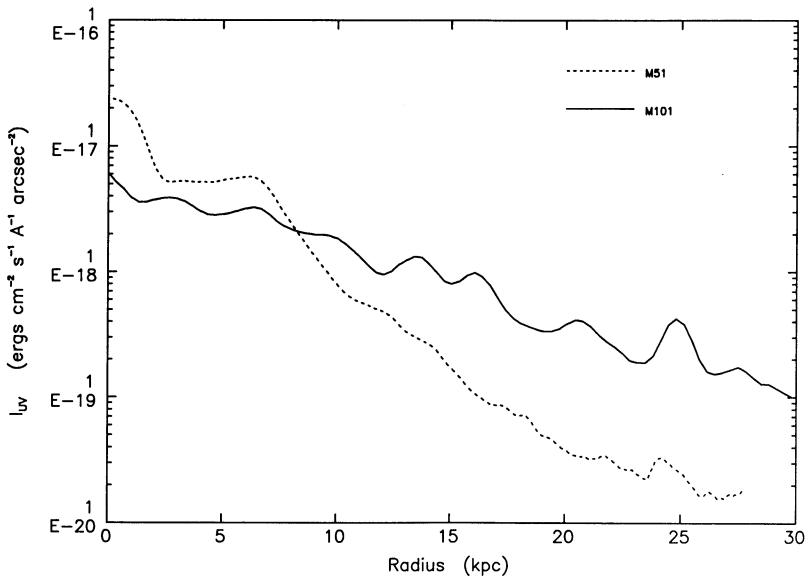

FIG. 9.—UV azimuthally averaged radial surface brightness profiles for M51 and M101. The M51 profile was extracted from the sum of the three 50 s exposures. Radial distances in kpc were computed assuming distances of 7.2 Mpc for M101 and 9.6 Mpc for M51.

IV. H II REGION PHOTOMETRY

CCM cataloged 161 H II regions in M51 identified from Hα interference filter images. Van der Hulst *et al.* (1988) determined radio continuum fluxes for a subset of the brighter H II regions from 6 cm and 20 cm VLA maps. They also measured Hα fluxes from digitized line and continuum plates, using apertures registered with the radio apertures. The radio fluxes at the two wavelengths allowed the separate determination of the thermal and nonthermal components. A constant spectral index of −0.9 was assumed for all nonthermal radio emission. The thermal emission was assumed to be optically thin, with a spectral index of −0.1. (The spectral index α is defined so that the radio flux S is proportional to ν^{α}.) They then estimated A_v by comparing the intrinsic ratio of the 6 cm thermal flux to the Hα flux with the observed ratio.

For 11 H II regions van der Hulst *et al.* also performed spectrophotometric measurements of Hα and Hβ fluxes. For these sources they determined A_v using the observed Balmer decrement compared with the theoretical value for zero extinction. They found that A_v (radio) exceeded A_v (Balmer) by about 0.5 magnitude on average, independent of A_v, concluding that most of the extinction does not take place either in opaque clumps (which would give gray wavelength independent extinction) or in homogeneous dust mixed with the ionized gas. A model in which the extinction takes place in a slab exterior to the H II region, with no significant scattering into the beam, together with 0.5 magnitude of gray extinction is consistent with their radio and optical data. For these extended sources, a gray extinction of 0.5 magnitude is equivalent to simply covering a fraction $1.0 \times 10^{(-0.4 \times 0.5)} = 0.37$ of the Hα emission inferred from the thermal radio flux with material which is perfectly opaque at UV and optical wavelengths, but transparent in the radio.

We measured UV and U fluxes in 14″ apertures for 17 H II regions observed by van der Hulst *et al.* (1988) with Hα fluxes greater than 8.0×10^{-14} ergs (cm^2 Å s)$^{-1}$. We calculated the positions of the H II regions on the images from the polar coordinates given in CCM, using the plate solutions determined from the Space Telescope Guide Stars positions (Lasker and McLean 1987). The measured UV and *U* fluxes of these H II regions are given in Table 1, along with F_{uv}/F_u colors and the A_v values of van der Hulst *et al.* We did not adjust the positions to center on the UV source nearest the H II region, but these bright uncrowded H II regions generally correspond with UV and *U* sources contained within the aperture.

TABLE 1

UV FLUXES, FLUX RATIOS, AND REDDENINGS FOR M51 H II REGIONS

CCM	log F_{uv}	log F_u	log (F_{uv}/F_u)	A_v
1	−15.01	−14.80	−0.21	2.61
5	−14.78	−14.69	−0.085	2.19
8	−14.74	−14.55	−0.20	1.26
9	−15.23	−15.25	0.026	2.26
10	−14.56	−14.45	−0.11	1.01
24	−14.55	−14.46	−0.094	2.27
43B	−14.25	−14.22	−0.033	2.22
45	−15.06	−14.77	−0.30	2.27
49	−15.03	−14.63	−0.40	3.11
52	−14.87	−14.58	−0.29	2.23
55	−14.95	−14.79	−0.16	0.91
71	−14.65	−14.34	−0.31	1.64
72	−14.82	−14.42	−0.39	1.93
86	−14.80	−14.91	0.11	1.90
91	−14.53	−14.70	0.17	2.04
94	−15.50	−15.18	−0.32	1.77
103	−15.06	−15.13	0.072	1.68

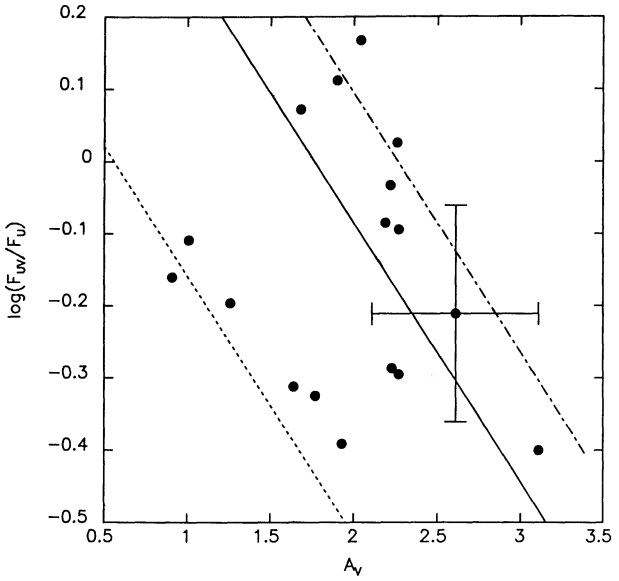

FIG. 10.—F_{uv}/F_u vs. *V* band extinction (from van der Hulst *et al.*) for 17 CCM H II regions with UV and *U* fluxes and extinction measurements. The solid line shows the expected relation for O-type stars reddened according to the Galactic extinction curve alone. The dash-dot line assumes 0.5 mag gray extinction. The dotted line assumes a cooler UV spectrum (T = 15,000 K) reddened by the Galactic extinction curve with no gray extinction.

The 17 tabulated F_{uv}/F_u H II region colors can be tested for consistency with simple extinction models. In Figure 10 we plot log (F_{uv}/F_u) versus A_v (radio). The solid line shows the expected dependence of log (F_{uv}/F_u) on A_v for the case in which all extinction takes place exterior to the H II region, and there is no clumping of the dust. The column density of absorbers is assumed to be uniform over the H II region. The Galactic extinction curve of Savage and Mathis (1979) determined the expected slope of the line, while the dereddened log (F_{uv}/F_u) for an O-type star with T_{eff} = 40,000 K (Kurucz 1979) determined the intercept value of 0.64.

The dot-dash line in Figure 10 represents the case in which 0.5 mag of the extinction A_v is wavelength-independent gray extinction. As explained earlier, in this case 37% of both the *U* and UV fluxes are assumed to be absorbed by opaque clumps or filaments. The F_{uv}/F_u flux ratio for a given A_v is then the same as for the zero-gray extinction case, with extinction A_v − 0.5. The points for 12 of the sample of 17 H II regions lie within the area bounded by the two lines to within the observational errors. We estimate the error in log (F_{uv}/F_u) at 0.15, while van der Hulst *et al.* estimate the error in A_v at 0.5. The five H II regions which lie below and to the left of the solid line (CCM 8, 10, 55, 71, and 72) have F_{uv}/F_u ratios too low to be consistent with a model in which both the UV and *U* fluxes are primarily from O stars, unless the A_v's have been systematically overestimated by at least a magnitude.

The discrepancy is only slightly reduced if the 6 cm flux observed by van der Hulst *et al.* is assumed to be entirely thermal. The F_{uv}/F_u colors of the five discrepant H II regions could be intrinsically redder than for the others because of e.g. a redder stellar population in addition to the O-type stars exciting the H II region. The lower dashed line is appropriate for the case where the zero-extinction value of log (F_{uv}/F_u) is

0.2, which is the value appropriate for a star of effective temperature about 15,000 K. Alternatively, A_v could have been underestimated because of e.g. missing 6 cm flux from compact components. The present data do not allow us to specify which (if either) of these explanations is correct. Four of the discrepant H II regions (CCM 10, 55, 71, and 72) have the four highest Hα fluxes of all the H II regions observed by van der Hulst *et al.*

V. THE NUCLEAR REGION OF M51

a) Summary of Recent Results

The inner arcmin of M51 has been the subject of a number of investigations in recent years, in a variety of bandpasses:

Worden (1974) used digitized images in the *B* and *V* bands to show that the nuclear region of M51 has a blue ring of diameter about 30″, with $B - V$ about 0.2. Pierce (1986) obtained CCD images of M51 in the *B*, *R*, and *I* passbands. He noted the nonaxisymmetric oval isophotes and suggested that such a mass distribution could result in noncircular streaming motions and enhanced star formation at the inner Lindblad resonance. Pierce identified this region with the blue ring of Worden.

Ford *et al.* (1985) found evidence for nonthermal activity in the nucleus, from Hα imagery and VLA radio continuum maps at 6 cm and 20 cm. Their 6 cm map shows a region of enhanced emission about 10–20 arcsec across. They attributed the morphology of this emission to the interaction of a nonthermal nuclear jet with ambient interstellar material. Goad and Gallagher (1985) and Cecil (1988) found that the N II emission lines in this region have widths of up to about 1500 km s^{-1}. They found evidence for a central nonstellar source of ionizing radiation and low-level Seyfert activity.

According to Palumbo *et al.* (1985) the nucleus is an extended source in the (2.0–4.0) keV band, and is brighter than the M83 nuclear source at X-ray wavelengths. They interpreted this emission as either from hot gas flowing out of the nucleus or as a starburst old enough to have X-ray emitting evolved binary systems.

The CO brightness temperature is a relative minimum at the position of the nucleus, according to the maps of Lo *et al.* (1987) and Rydbeck, Hjalmarson, and Rydbeck (1985). Turnrose (1976) found M51 to be unique among the seven Sc galaxy nuclei whose optical spectra he observed and modeled, in that his best-fit population model for the central 7″ included no unobscured O stars. This conclusion is consistent with the *IUE* spectrum obtained by Benvenuti and d'Odorico (1980). Turnrose suggested that star formation is prevented in the nucleus of M51 by the inner Lindblad resonance, which does not allow the spiral arms to propagate into the nucleus. He deduced the presence of an inner Lindblad resonance from the observed differential rotation.

Telesco, Decher, and Gatley (1986) performed an infrared east-west scan across the nucleus at a wavelength of 10 μm using a 9″ diameter beam. The 10 μm emission is not strongly peaked at the nucleus, but is distributed among several condensations over the inner arcmin. Telesco, Decher, and Gatley concluded that the dust responsible for the emission is heated predominantly by young stars, although they noted that the dust detected in the central 9″ may be heated by a nuclear nonthermal source.

Lester, Harvey, and Joy (1986) scanned across the nucleus at a wavelength of 100 μm. Using "superresolution" techniques they showed that the far-IR emission is bimodal, with two peaks separated by about 20″. They concluded that their scan is a cut across a ring, which they associated with the inner Lindblad resonance. They suggested that star formation is enhanced in the ring compared to the center.

b) Contour Maps from UV, U, and R Images

Figure 11*a*–11*c* show contour maps of the nuclear region constructed from our 6 s UV exposure, our 270 s *U* exposure, and our 180 s *R* band exposure.

Our 6 s UV exposure shows a clumpy region of UV emission which appears to coincide with the blue ring seen by Worden (1974). The ring is about 20–30 arcsec in diameter and is inclined like the nuclear ovals discussed by Pierce (1986). This is illustrated in Figure 11*a*. The UV emission peaks in two extended clumps, one east of the nucleus, the other to the west. The position of the nucleus is a relative minimum of the UV emission. The two clumps each have UV aperture fluxes about 3.6×10^{-15} ergs (cm^2 Å $s)^{-1}$, measured using apertures of radius 12″. Centering the aperture on the nucleus gives a UV flux lower by a factor 2. The bright H II region CCM 71 has about the same UV flux as the nuclear clumps, when measured with the same size aperture. The UV clumps are probably associated with the "ring of normal H II regions" in region 6 of Goad and Gallagher (1985).

The clumpy morphology of the nuclear UV emission probably coincides with the blue ring found by Worden (1974). Formation of massive stars is not now occurring at the nucleus itself, as evidenced by the minimum of UV emission, the *IUE* spectrum, and the spectrum synthesis results of Turnrose (1976). Oval perturbations to the gravitational potential may have caused most of the gas to collect near the inner Lindblad resonance, where star formation is now occurring. The nonthermal activity observed in the inner regions could be fueled by mass loss from the evolved giants of the bulge population. The two UV bright H II regions to the east are also prominent on the *U* band contour plot. The inner regions of the *U* image are dominated by the nuclear bulge source, which is not present in the UV image.

A comparison of the colors of the M51 nuclear bulge region with the color of M31's bulge and with star-forming regions in the spiral arms is of interest. Combining UV measurements by Bohlin *et al.* (1985) with aperture photoelectric photometry of M31 by Sandage, Becklin, and Neugebauer (1969), we find that $I_{uv}/I_u = 0.055$ and $I_u/I_r = 0.23$ for M31 in a 7″ aperture, after dereddening with the Savage and Mathis (1979) reddening curve assuming $E(B - V) = 0.10$. Using the Schweizer 17″.8 calibration aperture centered on the M51 nucleus, we find $I_{uv}/I_u = 0.26$ and $I_u/I_r = 0.39$. If we assume that the stellar population in the M51 bulge is a younger population added to an old bulge population like that in M31, and that all of the *R* band emission is from the old population, then we can subtract the contribution of the old population to the UV and *U* bands by scaling the *R* band flux appropriately. After subtracting the contribution of the old population, we find $I_{uv}/I_u = 0.85$ for the additional younger population in the M51 bulge, a typical value observed in the star-forming regions in the spiral arms. We conclude that stars are being formed in the UV bright "ring clumps" of the inner arcmin of M51, with characteristics similar to stars in the spiral arms, but possibly not in the inner 7″.

c) EW Scans through Nucleus: Comparison of UV, U, IR, CO

Figure 12 shows EW scans through the nuclear region as compiled from a variety of sources: our 6 s rocket UV expo-

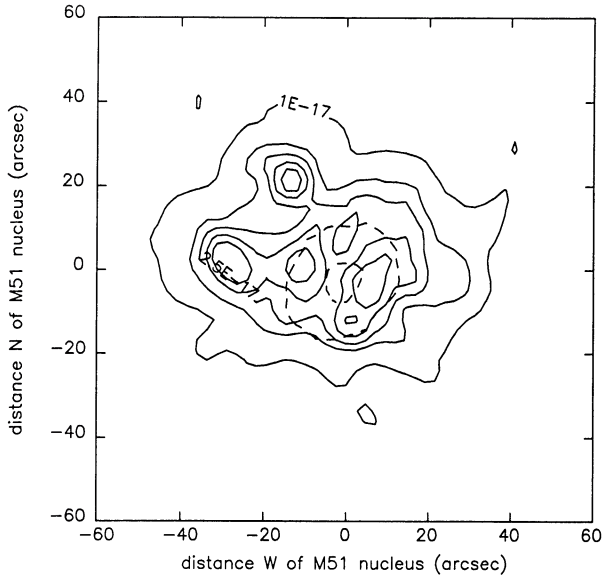

FIG. 11*a*

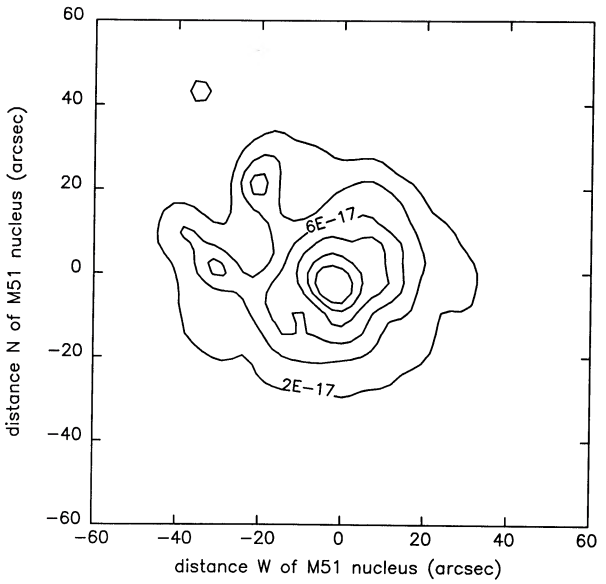

FIG. 11*b*

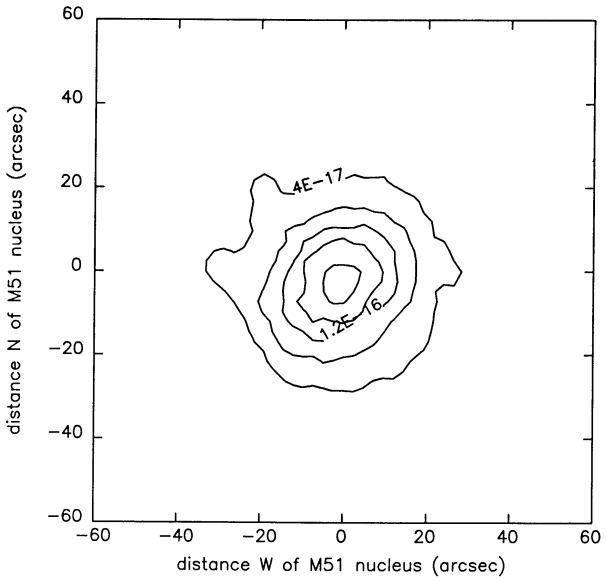

FIG. 11*c*

FIG. 11.—Surface brightness cntours for a 2′ × 2′ region centered on the M51 nucleus for the (*a*) UV; (*b*) *U*; and (*c*) *R* band images. Contour levels are: 1, 2, 2.5, 3, 3.5 (UV); 2, 4, 6, 8, 10, 12 (*U*); 4, 8, 12, 16, 32 (*R*) in units of $\times 10^{-17}$ ergs (cm^{2}Å s arcsec^2)$^{-2}$. The origin (0, 0) for these maps is at the coincident peaks of the *U* and *R* band images at $\alpha = 13^h29_m52^s9$, $\delta = 47°11'42''2$. The dashed contours on (*a*) are from the *R* band image, and show the offset of the *R* band nuclear maximum from the bright UV nuclear clumps and the coincidence of the UV clumps with the *R* band oval contours.

sure, our 270 s ground-based *U* band exposure, the 10 μm IR scan of Telesco, Decher, and Gatley (1986), and the 2.6 mm CO line map of Lo *et al.* (1987). All scans are given in arbitrary linear energy flux units. The *x*-axis is arcsec displacement from the nucleus. The UV and *U* data have been scaled by the same factor.

The UV scan has four major peaks distributed across the inner arcmin. None coincides with the nucleus, which is near the minimum between the two innermost peaks. These two inner peaks are about 20–25 arcsec apart, and are the two UV clumps discussed above. The far-eastern peak is associated with the H II region CCM 43B at the innermost extension of one of the spiral arms. The far-western peak is at the analogous position for another spiral arm.

The *U* scan shows three major sources, the brightest of which is at the position of the nucleus, and two "shoulders." The brightest source is similar to the de Vaucouleurs profile bulge typically seen in relatively inactive spiral bulges like that of M31. As in the case of M31, this component is from an old population. The bulge profile has "shoulders" at the positions of UV clumps. The outer peaks are the *U* counterparts of the inner spiral arm sources in the UV scan.

The 10 μm scan of Telesco, Decher, and Gatley shows relative maxima corresponding to four of the five *U* band peaks. The scan through the CO map shows peaks corresponding to the two spiral arm sources (the nuclear peak and UV clumps

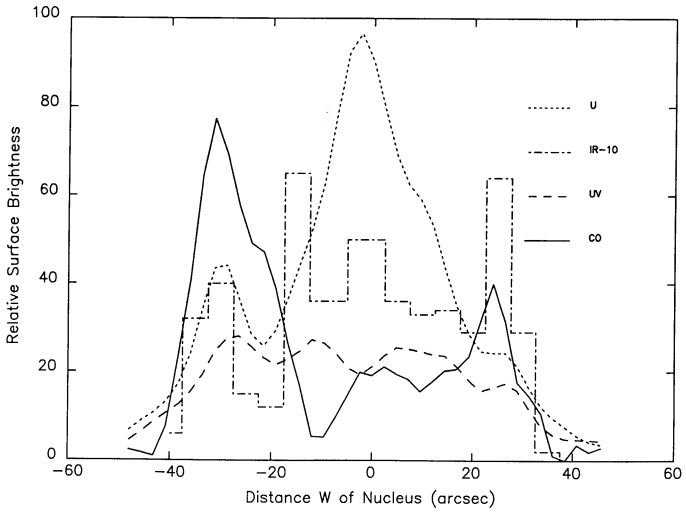

FIG. 12.—Relative surface brightness in UV, *U*, 10 μm IR (Telesco, Decher and Gatley) and CO (Lo *et al.*) for an E-W scan through the M51 nucleus.

are missing or inconspicuous). The two far-infrared (100 μm) peaks seen by Lester, Harvey, and Joy (1986) appear to be separated by about 20″, suggesting that they are associated primarily with the nuclear clumps also evident in the UV, rather than the spiral arm sources.

Although the inner arcminute of M51 was referred to as a "starburst" by Telesco, Decher, and Gatley, it is quite different in morphology from the starburst in M83. The M83 starburst is centrally condensed, with diameter about 100–200 pc, less than that of the star-formation ring near the center of M51 by about a factor of 5–10.

VI. NGC 5195

NGC 5195's barred appearance and recent interaction with M51 (Toomre and Toomre 1972) are both characteristics of galaxies with starburst nuclei. Our UV observations support the suggestion of Spinrad (1973) of such a starburst and permit us to compare it with M83, a similar case (Bohlin *et al.* 1983).

a) Extinction along the Line of Sight to NGC 5195's Nucleus

NGC 5195 is significantly redder than M51, which might result from extinction, an intrinsically red population, or both. Sandage (1961), Spinrad (1973), and Worden (1974) point out well-defined dust features from M51's northeast arm. Van Dyk (1987) detects Na I interstellar absorption in the direction of NGC 5195 at the velocity of M51 material in that arm. Spinrad's (1973) interpretation of spectra of NGC 5195 is that of a young (B star) population reddened by $E(B-V)$ of roughly 0.6, which he calls "inaccurate." Heckman (1980*a*) finds, from the relationship between continuum color and metallic line strength, an estimate of $\tau(\mathrm{H}\beta) \sim 3$ for the nuclear region.

Other published observations relevant to $E(B-V)$ in the direction of NGC 5195 are of low spatial resolution. Sage (1989) detects two features in the $J = 1 \rightarrow 0$ CO spectrum of NGC 5195: a narrow (FWHM ~ 60 km s^{-1}) component associated with the intervening arm of M51, and a wide (FWHM ~ 150 km s^{-1}) component associated with NGC 5195. We assume NGC 5195 is obscured by all material along the line of sight in M51's arm and half the material along the line of sight in NGC 5195's nucleus. Summing half the column density associated with the NGC 5195 feature and the column density associated with the M51 feature, calculated using the conversion of Scoville and Young (1983), gives a total molecular hydrogen column density of 2.7×10^{21} cm^{-2}, measured at an angular resolution of 55″. The H I observations of A. Rots (1989) imply N(H I) values ranging from 6×10^{20} cm^{-2} at the nucleus to 2–5 $\times 10^{20}$ cm^{-2} on the western edge of NGC 5195, measured at 34″ resolution. Constructing a total column density from the sum of the molecular and atomic hydrogen column densities at the nucleus of NGC 5195, using the gas-to-dust conversion of Bohlin, Savage, and Drake (1978) gives a reddening of $E(B-V) = 0.6$ mag, in agreement with Spinrad's value, measured at 0.5–1 arcmin angular resolution. Galactic extinction in the NGC 5195 direction is negligible.

b) The Stellar Population of NGC 5195's Nucleus

NGC 5195 has been described as a dwarf S0 galaxy (Burbidge and Burbidge 1964), an M82 irregular (Sandage 1961) and intermediate types; thus its stellar population is controversial, although this is undoubtedly due in large part to its uncertain reddening. Spinrad (1973) finds that his spectrum of NGC 5195 requires a population of stars as early in type as B5.

The F_{uv}/F_v ratio for NGC 5195's nucleus is 0.02, computed from photoelectric photometry in a 20″ aperture by Burkhead (1978) and UV photometry from a similar-sized aperture on our 6 s exposure. Correcting by the maximum reddening derived above, assuming $\mathrm{E(UV}-V)/E(B-V) = 4.4$, gives a corrected F_{uv}/F_v ratio of 0.19. For comparison the nucleus of M31 has a corrected F_{uv}/F_v ratio of 0.044 (1.6 mag redder). If the stellar population of NGC 5195's nucleus is intrinsically bluer than that of M31, as the optical spectroscopy of Spinrad implies, there must be significant reddening, consistent with the observations of interstellar gas discussed above. In addition, NGC 5195 is a reasonably bright infrared source (Smith 1982; Roche and Aitken 1985; Beck, Turner, and Ho 1986), implying the existence of both young stars and considerable internal dust.

Heckman and coworkers (Heckman, Balick and Crane 1980; Heckman 1980*a*, *b*) have employed spectrophotometric measurements to classify spectra of the nuclei of bright galaxies in order to determine their stellar populations and other properties. On the basis of a comparison of metal line and Balmer line ratios for such nuclei with H II regions Heckman (1980*a*) determines the stellar population of NGC 5195 to be of the "composite" type (containing a significant young component) with a "moderately strong" young population.

We conclude that the nucleus of NGC 5195, while obscured by dust both within the nucleus and along the line of sight, contains a significant young population (stars as early as B5).

c) Interpretation as a Starburst

Our previous work (Bohlin *et al.* 1983) identifying the nuclear starburst in M83 was based heavily on the striking appearance of M83's nucleus in the ultraviolet: a compact ($\sim$5–10 arcsec FWHM) source supplying 16%–20% of the entire galaxy's total UV flux. *IUE* observations revealed M83's UV spectrum to be similar to that of NGC 7714, a well-known starburst.

NGC 5195's nucleus, apparently obscured by internal and external dust, presents no such striking UV appearance. The UV nucleus is displaced by about half the UV FWHM to the east of the coincident U and R band nuclei. The 1.65 μm images of Gatley, DePoy, and Fowler (1988) clearly show a bright central condensation at the apparent position of the U and R band nuclei. Therefore, the UV appearance is most likely formed by a combination of foreground and internal dust and a bright compact nucleus. The color of the UV object, described above, is not remarkable. Unfortunately, NGC 5195 is too faint for *IUE* observations. The 2500 Å rocket flux is less than 1/200 that of M83's nuclear starburst, for which about $\frac{1}{2}$ hr exposure time is required for *IUE* exposures with acceptable S/N for either camera.

Our arguments for the starburst nature of NGC 5195 are based on broad-band fluxes in several bandpasses. In Table 2 we present a comparison of fluxes and luminosities from M83 and NGC 5195 over a large wavelength range. Where relevant the values are corrected to a distance to NGC 5195 of 9.6 Mpc and a distance to M83 of 3.75 Mpc.

NGC 5195 is slightly fainter in the radio wavelength region, much fainter in the UV, and brighter in the X-ray region, when compared with M83. In the infrared, strong spectral differences are apparent: at long wavelengths (>100 μm) NGC 5195 is much fainter, while the two sources are comparable at 12 μm. Smith (1982) computes, from 70, 110, and 170 μm data, a dust temperature of 55–65 K and a dust total IR luminosity of

TABLE 2

COMPARISON OF NGC 5195 WITH M83

Wavelength	NGC 5195	Ref.	M83	Ref.
X-ray (0.2–4 keV, erg s^{-1})	2.1×10^{39}	1	1×10^{39}	2
F_{uv}(2500 Å)[ergs (cm^2 Å s)$^{-1}$] (@9.6 Mpc; no reddening correction)	1.0×10^{-15}	3	3.6×10^{-14}	4
12 μm [$W/(cm^2 \mu)$]	4.7×10^{-19}	5	7.5×10^{-19}	5
25 μm (Jy)	1.55	6	19.6	6
60 μm (Jy)	10.0	6	104	6
70 μm (Jy)	24	8		
83 μm (Jy)	...	...	131	7
100 μm (Jy)	<1.0	6	214	6
110 μm (Jy)	12.4	8		
170 μm (Jy)	6.1	8		
Total far-IR ($L_\odot$)	3×10^9	8	3×10^9	7
20 cm (mJy)	61	9	100	10

REFERENCES.—(1) Palumbo *et al.* 1985; (2) Fabbiano, Trinchieri, and MacDonald 1983; (3) Present paper; (4) Bohlin *et al.* 1983; (5) Roche and Aitken 1985; (6) *IRAS* Point Source Catalog; (7) Telesco and Harper 1980; (8) Smith 1982; (9) Segalowitz 1977; (10) Condon *et al.* 1985.

3×10^9 $L_\odot$, equal to that of M83. Therefore, NGC 5195 displays all the characteristics of a strong starburst like M83's except that its UV flux is too small by about a factor 40. This lack is easily explained by dust, partly mixed with the starburst, and partly intervening along the line of sight, presumably in a region of small (<30″) extent.

Other aspects of the data strongly suggest abnormal dust distribution. Smith (1982) and Beck, Turner, and Ho (1986) explain the infrared and radio emission by invoking relatively small amounts of dust (3×10^4 $M_\odot$) at relatively high temperatures. However, this claim applies only to dust actually radiating strongly at 10–170 μm; the amount of dust present in the nuclear region of NGC 5195 may be much larger. For example, dust at 5 K radiates at 170 μm (the longest observed IR wavelength) 10^4 times less strongly, per unit radiating area, than dust at 65 K. The geometry implied by the infrared and UV data places the strongly radiating hot dust nearer to the illuminating stars than in comparable (IC 342, M83, NGC 253: see Roche and Aitken 1985) starburst nuclei; additional dust is farther away and shielded from UV radiation, so it remains cold.

We conclude that the nucleus of NGC 5195 contains a starburst that is quantitatively similar to that of M83. Apparent differences may be explained by a different distribution of stars and dust, specifically leading to smaller UV flux and an infrared spectrum dominated by radiation from hotter dust.

VII. SUMMARY

UV images of the M51 system were obtained with a rocket-borne telescope in a band centered at about 2500 Å with spatial resolution about 10″. Ground-based images in the *U* and *R* bands were obtained for comparison.

UV emission of the system is dominated by an extended nuclear source, with structure correlated with similar structures seen in other bands, and by a complex of bright H II regions in the northeast bright spiral arm. Each of these components contributes about 20% of the UV emission of the system. Radial profiles cannot be fitted by single power laws in any of the bands. UV azimuthal profiles show structure identifiable with bright H II regions discovered in Hα imagery, as previously found in the case of M101 (Hill, Bohlin, and Stecher 1984).

Most bright H II regions with extinctions determined from radio and Hα flux measurements have F_{uv}/F_u colors consistent with O stars reddened by those amounts. Some of the brightest H II regions show evidence for a composite population, with significant contributions from cooler stars.

Though apparently faint in the UV, the interacting companion NGC 5195 is significantly reddened, and probably contains a starburst comparable to that previously found in M83 (Bohlin *et al.* 1983).

The ground-based images were obtained by Michael N. Fanelli with the assistance of Dean Ketelsen. We thank Dr. K. Y. Lo for providing a CO map of M51, and Dr. A. Rots for providing information from H I data in advance of publication.

The funding for this research was through NASA RTOP 680-879-11-41, NASA Spacelab Project 680-440-51-02 and NASA grant NAG-5-700 (R.W.O.).

REFERENCES

Beck, S. C., Turner, J. L., and Ho, P. T. P. 1986, *Ap. J.*, **309**, 70.
Benvenuti, P., and d'Odorico, S. 1980, in *The Universe at Ultraviolet Wavelengths: the First Two Years of International Ultraviolet Explorer*, (*NASA Conf. Pub. 2171*), p. 725.
Bohlin, R. C., Cornett, R. H., Hill, J. K., Hill, R. S., O'Connell, R. W., and Stecher, T. P. 1985, *Ap. J. (Letters)*, **298**, L37.
Bohlin, R. C., Cornett, R. H., Hill, J. K., Smith, A. M., and Stecher, T. P. 1983, *Ap. J. (Letters)*, **274**, L53.
Bohlin, R. C., Hill, J. K., Stecher, T. P., and Witt, A. N. 1982, *Ap. J.*, **255**, 87.
Bohlin, R. C., Savage, B. D., and Drake, J. F. 1978, *Ap. J.*, **224**, 132.
Boroson, T. 1981, *Ap. J. Suppl.*, **46**, 177.
Burbidge, E. M., and Burbidge, G. R. 1964, *Ap. J.*, **140**, 1445.
Burkhead, M. S. 1978, *Ap. J. Suppl.*, **38**, 147.
Carranza, G., Crillon, R., and Monnet, G. 1969, *Astr. Ap.*, **1**, 479 (CCM).
Cecil, G. 1988, *Ap. J.*, **329**, 38.
Condon, J. J., Condon, M. A., Gisler, G., and Puschell, J. J. 1982, *Ap. J.*, **252**, 102.
Cornett, R. H., Hill, J. K., and Hill, R. S. 1987, *UIT Batch Data Reduction: Data and Programs* (Lanham, MD: ST Systems Corporation; STX-T-25-3002-0007-87).
Elmegreen, D. M., and Elmegreen, B. G. 1984, *Ap. J. Suppl.*, **54**, 127.
Fabbiano, G., Trinchieri, G., and MacDonald, A. 1983, *Bull. AAS*, **14**, 948.
Ford, H. C., Crane, P. C., Jacoby, G. H., Lawrie, D. G., and van der Hulst, J. M. 1985, *Ap. J.*, **293**, 132.
Gatley, I., DePoy, D. L., and Fowler, A. M. 1988, *Science*, **242**, 1264.
Goad, J. W., and Gallagher, J. S. 1985, *Ap. J.*, **297**, 98.
Heckman, T. M. 1980*a*, *Astr. Ap.*, **87**, 142.
———. 1980*b*, *Astr. Ap.*, **87**, 152.

Heckman, T. M., Balick, B., and Crane, P. C. 1980, *Astr. Ap. Suppl.*, **40**, 295.
Hill, J. K., Bohlin, R. C., and Stecher, T. P. 1984, *Ap. J.*, **277**, 542.
Hill, R. S. 1987, *UIT Batch Data Reduction: Design and Maintenance* (Lanham, MD: ST Systems Corporation; STX-T-25-3002-0008-87).
Joint *IRAS* Science Working Group 1988, *The IRAS Point Source Catalog*, (NASA Ref. Pub. RP-1190).
Kormendy, J., and Norman, C. A. 1979, *Ap. J.*, **233**, 539.
Kurucz, R. L. 1979, *Ap. J. Suppl.*, **40**, 1.
Landsman, W. B., and Pfarr, B. B. 1989, in preparation.
Lasker, B. M. and McLean, B. 1987, private communication.
Lester, D. F., Harvey, P. M., and Joy, M. 1986, *Ap. J.*, **302**, 280.
Lo, K. Y., Ball, R., Masson, C. R., Phillips, T. G., Scott, S., and Woody, D. P. 1987, *Ap. J. (Letters)*, **317**, L63.
Palumbo, G. G. C., Fabbiano, G., Fransson, C., and Trinchieri, G. 1985, *Ap. J.*, **298**, 259.
Pierce, M. D. 1986, *A.J.*, **92**, 287.
Richter, O.-G., and Rosa, M. 1989, *Astr. Ap.*, **206**, 219.
Roche, P. F., and Aitken, D. K. 1985, *M.N.R.A.S.*, **213**, 789.
Rots, A. 1989, private communication.
Rydbeck, G., Hjalmarson, A., and Rydbeck, O. E. H. 1985, *Astr. Ap.*, **144**, 282.
Sage, L. J. 1989, preprint.
Sandage, A. R. 1961, *The Hubble Atlas of Galaxies* (Washington: Carnegie Institution of Washington).
Sandage, A. R., Becklin, E. E., and Neugebauer, G. 1969, *Ap. J.*, **157**, 55.
Sandage, A. R., and Tammann, G. A. 1974, *Ap. J.*, **194**, 559.
Savage, B. D., and Mathis, J. S. 1979, *Ann. Rev. Astr. Ap.*, **17**, 73.
Schweizer, F. 1976, *Ap. J. Suppl.*, **31**, 313.
Scoville, N. Z., and Young, J. S. 1983, *Ap. J.*, **265**, 148.
Segalowitz, A. 1977, *Astr. Ap.*, **54**, 703.
Smith, J. 1982, *Ap. J.*, **261**, 463.
Spinrad, H. 1973, *Ap. J.*, **182**, 381.
Stecher, T. P., Bohlin, R. C., Hill, J. K., and Jura, M. A. 1982, *Ap. J. (Letters)*, **255**, L99.
Stetson, P. B. 1987, *Pub. A.S.P.*, **99**, 191.
Telesco, C. M., Decher, R., and Gatley, I. 1986, *Ap. J.*, **302**, 632.
Telesco, C. M., and Harper, D. A. 1980, *Ap. J.*, **235**, 392.
Toomre, A., and Toomre, J. 1972, *Ap. J.*, **178**, 623.
Turnrose, B. E. 1976, *Ap. J.*, **210**, 33.
van der Hulst, J. M., Kennicutt, R. C., Crane, P. C., and Rots, A. H. 1988, *Astr. Ap.*, **195**, 38.
van Dyk, S. D. 1987, *Pub. A.S.P.*, **99**, 467.
Worden, S. P. 1974, *Pub. A.S.P.*, **86**, 92.

RALPH C. BOHLIN: Space Telescope Science Institute, Homewood Campus, Baltimore, MD 21218

ROBERT H. CORNETT and JESSE K. HILL: ST Systems Corporation, 4400 Forbes Blvd., Lanham, MD 20706

ROBERT W. O'CONNELL: Leander McCormick Observatory, University of Virginia, P.O. Box 3818, University Station, Charlottesville, VA 22903-0818

THEODORE P. STECHER: Laboratory for Astronomy and Solar Physics, NASA/Goddard Space Flight Center, Code 680, Greenbelt, MD 20771